Electrochimica Acta 95 (2013) 87–94

Contents lists available at SciVerse ScienceDirect

Electrochimica Acta

journal homepage: www.elsevier.com/locate/electacta

Synthesis and electrochemical performance of long lifespan Li-rich $Li_{1+x}(Ni_{0.37}Mn_{0.63})_{1-x}O_2$ cathode materials for lithium-ion batteries

Min Gao, Fang Lian*, Hongquan Liu, Cuijun Tian, Leilei Ma, Wangyue Yang

School of Materials Science and Engineering, University of Science and Technology Beijing, Beijing 100083, PR China

ARTICLE INFO

Article history:
Received 6 October 2012
Received in revised form 31 January 2013
Accepted 31 January 2013
Available online 14 February 2013

Keywords:
Lithium-ion battery
Cathode materials
Lithium-rich
Cycle stability

ABSTRACT

$Li_{1+x}(Ni_{0.37}Mn_{0.63})_{1-x}O_2$ (x = 0.123, 0.111, 0.086, 0.070, 0.031) cathode materials were synthesized via coprecipitation of carbonates and the samples with long lifespan for lithium ion batteries were obtained through adjusting the content of lithium. Their crystal structure and electrochemical performance were characterized by means of powder X-ray diffraction (XRD), field emission scanning electron microscopy (FESEM), inductive coupled plasma (ICP), galvanostatic charge/discharge test and electrochemical impedance spectrum (EIS). The XRD data show that the materials can be indexed as a single α-$NaFeO_2$ phase except the sample with x = 0.031. The FESEM results indicate that the primary particles size increase with an increase of x value and the secondary particles retain the spherical morphology. The as-prepared sample with x = 0.086 delivers the largest discharge capacity of 232.1 mAh g^{-1} and a high initial efficiency of 81.8% at 0.2 C in the potential range of 2.5–4.7 V. Moreover, the better cycle performances are obtained for samples with x = 0.123 and 0.111, and the capacity retentions are up to 89 and 81% of the first discharge capacity at 0.5 C after 500 cycles, respectively.

1. Introduction

Recently, lithium- and manganese-rich $Li[Li_{1-x-y}Me_xMn_y]O_2$ (Me = Co [1–3], Cr [4], Ni [5–7], NiCo [8,9], etc.) compounds have become attractive cathode materials owing to their high capacity (>250 mAh g^{-1}) and cheaper raw material [5,7,10]. Generally, $Li[Li_{1-x-y}Me_xMn_y]O_2$ can be recognized as a solid solution of Li_2MnO_3 and $LiMeO_2$, which have a similar structural model as O_3-$LiCoO_2$ (space group $R\bar{3}m$), except for the superlattice structure [11–13]. $Li[Li_{1-x-y}Me_xMn_y]O_2$ can obtain an enhanced structural stability at high charged state and additional capacity at high voltage beyond 4.5 V vs. Li/Li^+ from the integrated Li_2MnO_3. However, $Li[Li_{1-x-y}Me_xMn_y]O_2$ suffers from a large initial irreversible capacity loss (50–100 mAh g^{-1}) [11,14–16], inferior rate capability, poor cycle life and a significant decrease of the discharge voltage plateau upon cycling [17–20]. Some strategies have been proposed to overcome these issues. Johnson et al. [21] reported that acid treatment can greatly lower the first-cycle irreversible capacity loss of the $Li[Li_{1-x-y}Me_xMn_y]O_2$ electrodes. A. Manthiram et al. [22,23] realized the high initial coulombic efficiency by blending $Li[Li_{1-x-y}Me_xMn_y]O_2$ with some insertion host materials, such as V_2O_5, VO_x, $Li_4Mn_5O_{12}$ and so on. Although the initial irreversible capacity can be reduced by the above approaches, the cycleability and rate capability of $Li[Li_{1-x-y}Me_xMn_y]O_2$ were deteriorated in the cases, which can be mitigated by cobalt incorporated or surface modification [24,25]. Nevertheless, few report, to our knowledge, shows the successful improvement on its integrated properties, such as high initial efficiency, good rate capability, long cycle life (i.e. 500 cycles) and suppressed decline of discharge voltage plateau especially after long-term cycling.

With the aim of achieving a high-performance of Li-rich materials, we synthesized the $Li_{1+x}(Ni_{0.37}Mn_{0.63})_{1-x}O_2$ (x = 0.123, 0.111, 0.086, 0.070, 0.031) cathode materials from $Ni_{0.37}Mn_{0.63}CO_3$ carbonate precursor, and the effects of lithium content on the integrated electrochemical performance were studied, including initial efficiency, rate capability, the change of discharge voltage plateau and long cycling behavior.

2. Experimental

$LiOH{\cdot}H_2O$, $Ni(NO_3)_2{\cdot}6H_2O$ (all are 99.9% in purity) and $Mn(NO_3)_2$ (50% aqueous solution) were used as the starting materials for the synthesis of $Li_{1+x}(Ni_{0.37}Mn_{0.63})_{1-x}O_2$ (x = 0.123, 0.111, 0.086, 0.070, 0.031). A mixed aqueous solution of 2.0 M transition metal nitrate and 2.0 M Na_2CO_3 solution were simultaneously added dropwise by peristaltic pump into a reactor, in which distilled water was under vigorous stirring. The pH value in the reactors was maintained at 8.2, while the temperature was held at 60 °C. The resulting precipitates were filtered and washed three times to remove residual Na^+, and then dried under nitrogen at

* Corresponding author. Tel.: +86 1082377985; fax: +86 1082377985.
E-mail addresses: lianfang@mater.ustb.edu.cn, ustbenergy@yahoo.cn (F. Lian).

0013-4686/$ – see front matter © 2013 Elsevier Ltd. All rights reserved.
http://dx.doi.org/10.1016/j.electacta.2013.01.159

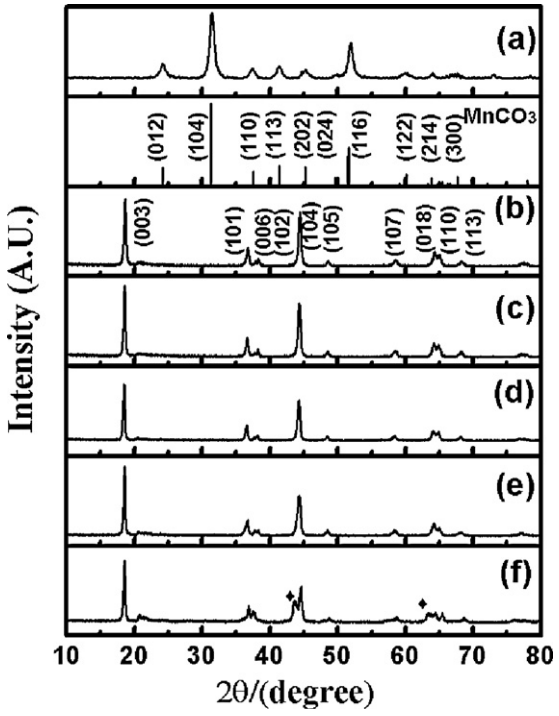

Fig. 1. XRD patterns of (a) the $(Ni_{0.37}Mn_{0.63})CO_3$ precursor and (b–f) the $Li_{1+x}(Ni_{0.37}Mn_{0.63})_{1-x}O_2$ samples: (b) $x = 0.123$; (c) $x = 0.111$; (d) $x = 0.086$; (e) $x = 0.070$; (f) $x = 0.031$ (the symbol ♦ denotes peaks assigned as Fm-3m).

120 °C over 24 h. The as-obtained precursor was subsequently mixed with $LiOH{\cdot}H_2O$ using mortar and pestle. The mixture was preheated at 450 °C for 6 h, then grinded and finally sintered at 850 °C for 12 h in muffle furnace under air.

Powder X-ray diffraction (Rigaku D/max, Japan) using Cu K radiation was used to identify crystalline phase of the as-prepared samples. FESEM analysis was performed using ZEISS supra55 field emission scanning electron microscope (Germany). Particle size distribution was estimated by laser size distribution measurements LMS-30 (Japan fresh Co., Ltd.). The precise cation composition of the samples was determined by inductively coupled plasma optical emission spectroscopy (Spectroflame ICP, 2.5 kW, 27 MHz).

The positive electrodes for the electrochemical studies were prepared in the form of thin films of a mixture of $Li_{1+x}(Ni_{0.37}Mn_{0.63})_{1-x}O_2$, acetylene black, and polyvinylidene fluoride (PVDF) binder (in a 85:10:5 weight ratio) coated onto aluminum foil. The as-fabricated electrodes were dried at 120 °C and then cut into 12 mm in diameter. Coin cells (CR2032) were assembled and sealed in an argon-filled glove box with 1 M $LiPF_6$ dissolved in EC/DMC/DEC (1:1:1 in volume rate) as electrolyte, metallic lithium and porous polypropylene films as anode and separator, respectively. Charge and discharge tests were all performed galvanostatically between 2.5 and 4.7 V at 25 °C at different rates (1 C rate corresponds to the current density of 200 mAg^{-1}) with a LAND CT2001A battery test system (Jinnuo Wuhan Corp., China). Electrochemical impedance spectrum (EIS) was performed under a frequency range 100 kHz–0.001 Hz using a vibration voltage of 5 mV to determine the resistance of the cycled cells.

3. Results and discussion

Powder XRD patterns of the co-precipitated $(Ni_{0.37}Mn_{0.63})CO_3$ precursor and $Li_{1+x}(Ni_{0.37}Mn_{0.63})_{1-x}O_2$ ($x = 0.123$, 0.111, 0.086, 0.070, 0.031) materials are shown in Fig. 1(a–g). As shown in Fig. 1(a), the XRD pattern fits well with the structure of $MnCO_3$ (rhodochrosite, R-3c, JCPDS No.44-1472) and no remarkable secondary phase can be observed under the resolution of the diffractometer, which indicates the complete intersolubility of $MnCO_3$ and $NiCO_3$. Moreover, the broadness of the diffraction peaks could be attributed to the small grain size of the primary particles with the value of about 8 nm calculated by the Scherrer equation [26]. $Li_{1+x}(Ni_{0.37}Mn_{0.63})_{1-x}O_2$ ($x = 0.123$, 0.111, 0.086, 0.070, 0.031) materials were synthesized by a high-temperature calcination process after thoroughly mixing the corresponding carbonate precursor with $LiOH{\cdot}H_2O$. From Fig. 1(b-f), we can see that the major peaks in all $Li_{1+x}(Ni_{0.\ 37}Mn_{0.63})_{1-x}O_2$ samples can be indexed based on a hexagonal a-$NaFeO_2$ structure (space group: R-3m, No.166). Meanwhile, the weak reflection peaks between 20 and 25° can be observed, which correspond to the superlattice ordering of Li, Ni and Mn in the transition metal layers for the Li-rich layered solid solution materials [6–8]. The details of the atomic arrangement in the transition metal layers of these materials are not confirmed yet [27]. In addition, the XRD pattern of $Li_{1.031}(Ni_{0.37}Mn_{0.63})_{0.969}O_2$ ($x = 0.031$) shows some slight peaks (marked with ♦ in Fig. 1e) which can be assigned as cubic rock-salt structure impurity component Ni_6MnO_8 (space group: Fm-3m, No. 225). The as-obtained material separates into a cubic rock-salt phase and a dominated layered phase with lack of lithium in agreement with the previous reports on the layered cathode materials [28,29]. Furthermore, the splitting of the diffraction peaks (0 0 6)/(1 0 2) and (1 0 8)/(1 1 0) in the XRD patterns become weak with decreasing of Li excessive value *x*.

Table 1
The experimental and theoretical results of Ni/Mn and Li/(Ni + Mn) ratios of the $(Ni_{0.37}Mn_{0.63})CO_3$ precursor and the $Li_{1+x}(Ni_{0.37}Mn_{0.63})_{1-x}O_2$ materials.

Sample	Ni/Mn		Li/(Ni + Mn)	
	Experimental	Theoretical	Experimental	Theoretical
Precursor	0.585	0.587	–	–
$x = 0.123$	0.585	0.587	1.230	1.281
$x = 0.111$	0.587	0.587	1.256	1.25
$x = 0.086$	0.587	0.587	1.203	1.188
$x = 0.07$	0.586	0.587	1.169	1.151
$x = 0.031$	0.586	0.587	1.093	1.064

The nominal compositions of the $(Ni_{0.37}Mn_{0.63})CO_3$ precursor and $Li_{1+x}(Ni_{0.37}Mn_{0.63})_{1-x}O_2$ ($x = 0.123$, 0.111, 0.086, 0.070, 0.031) samples were confirmed by the ICP/OES elemental analysis technique. As presented in Table 1, the results indicate that the average chemical compositions of the obtained materials are very close to the targeted stoichiometry.

Fig. 2(a–h) shows the SEM images of co-precipitated $(Ni_{0.37}Mn_{0.63})CO_3$ precursor and $Li_{1+x}(Ni_{0.37}Mn_{0.63})_{1-x}O_2$ ($x = 0.123$, 0.111, 0.086, 0.070, 0.031) samples, as well as the result of particle size distribution of the $(Ni_{0.37}Mn_{0.63})CO_3$ precursor. As can be seen from Fig. 2(a–b), the co-precipitated precursor consists of roughly 20 μm spherical aggregates by primary particles with diameters ≤100 nm, in agreement with the broaden diffraction peaks in the XRD patterns. Moreover, the as-prepared $(Ni_{0.37}Mn_{0.63})CO_3$ has a narrow diameter range with the average particle size of 17.353 μm. In addition, the secondary particles of the $Li_{1+x}(Ni_{0.37}Mn_{0.63})_{1-x}O_2$ samples retain the spherical morphology of $Ni_{0.37}Mn_{0.63}CO_3$ precursor, which are not shown here. We can see in Fig. 2(c–g) that the primary particles undergo a size decrease with the content of Li excessive value x decreasing. $Li_{1+x}(Ni_{0.37}Mn_{0.63})_{1-x}O_2$ samples with $x = 0.070$ and 0.031 consist of primary crystallites of 50–100 nm in diameter, while the particles of $Li_{1+x}(Ni_{0.37}Mn_{0.63})_{1-x}O_2$ with $x = 0.086$, 0.111 and 0.123 exhibit homogenous morphology around 100–200 nm in a well-shaped configuration. The results indicate that the content of excessive Li in the Li-rich series can improve the primary particles size and crystallization of $Li_{1+x}(Ni_{0.37}Mn_{0.63})_{1-x}O_2$ materials.

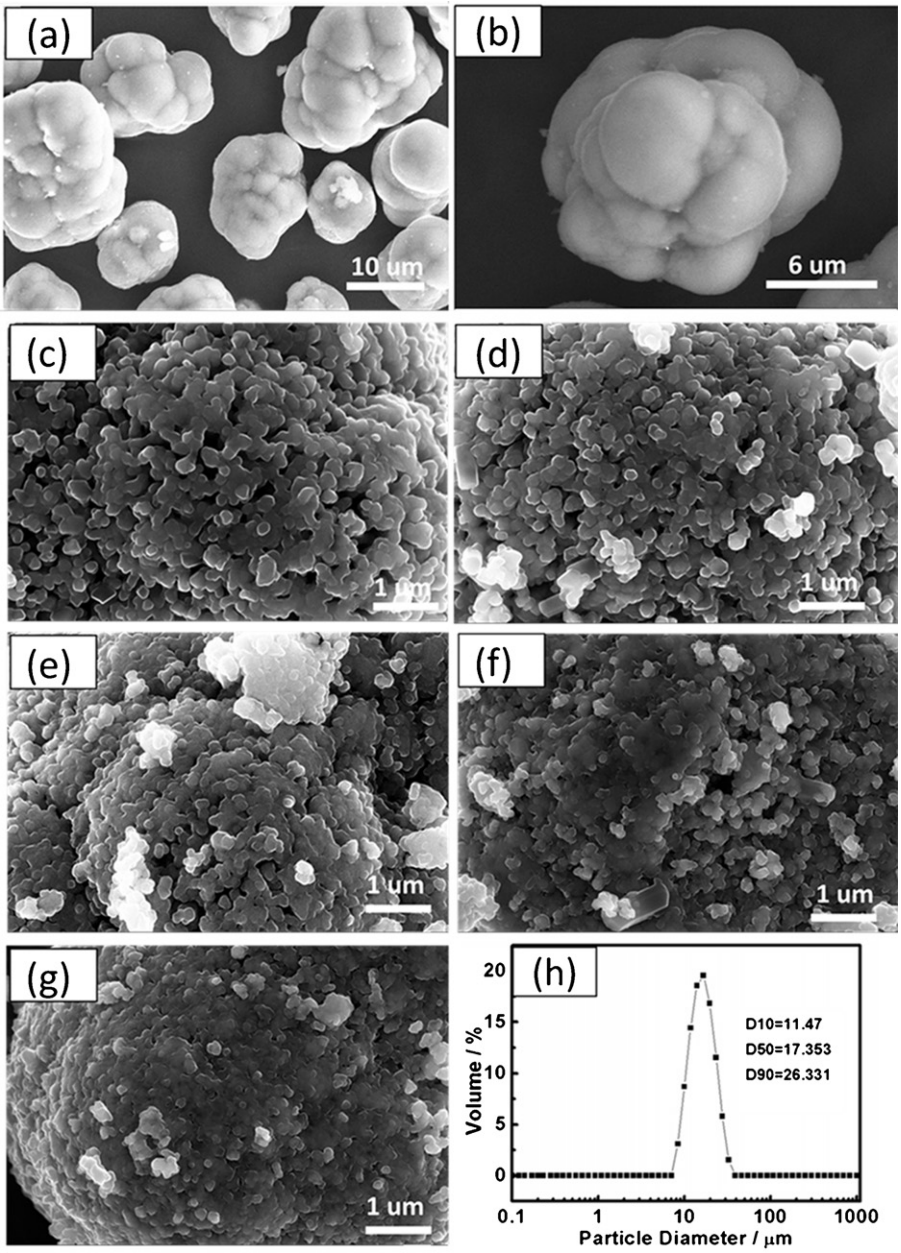

Fig. 2. SEM images of (a–b) the $(Ni_{0.37}Mn_{0.63})CO_3$ precursorand (c–g) the $Li_{1+x}(Ni_{0.37}Mn_{0.63})_{1-x}O_2$ samples: (c) $x = 0.123$; (d) $x = 0.111$; (e) $x = 0.086$; (f) $x = 0.070$; (g) $x = 0.031$. (h) Particle size distribution of the $(Ni_{0.37}Mn_{0.63})CO_3$ precursor.

Fig. 3(a) shows the initial charge/discharge voltage profiles of the $Li_{1+x}(Ni_{0.37}Mn_{0.63})_{1-x}O_2$ electrodes in the potential range of 2.5–4.7 V at 0.2 C, while the initial discharge capacity/initial efficiency with excessive lithium content x are demonstrated in Fig. 3(b). During the initial charge to 4.7 V, the electrochemical reaction occurs in two dominant stages: a smoothly sloping voltage profile below 4.5 V, which is attributed to the removal of lithium from the electrode structure accompanied with the oxidation of Ni^{2+} to Ni^{4+}, and the voltage plateau profile above 4.5 V, which could be ascribed to the activation of Li_2MnO_3 component [18,30]. This activation process has been considered to be associated with the irreversible extraction of Li_2O from the transition metal oxide composite materials [31]. The initial discharge capacity and efficiency values increase for the samples with $x = 0.123$ decrease to 0.070, and then decreased when the x value for the samples decreases from 0.070 to 0.031 sequentially (Fig. 3(b)). As shown in Fig. 3(a), $Li_{1.031}(Ni_{0.37}Mn_{0.63})_{0.969}O_2$ ($x = 0.031$) electrode exhibits higher charge voltage plateau and lower discharge voltage plateau than other samples, which indicates the larger polarization of $Li_{1.031}(Ni_{0.37}Mn_{0.63})_{0.969}O_2$ ($x = 0.031$) when charged and discharged at 0.2 C. However, $Li_{1.086}(Ni_{0.37}Mn_{0.63})_{0.914}O_2$ ($x = 0.086$) delivers the largest discharge capacity of 232.1 mAh g^{-1} and a high initial efficiency is 81.8% at 0.2 C between 2.5 and 4.7 V, which is contributed to small primary particles and high crystallinity from a textural point of view [32,33]. Hence, it is believed that the lithium content contributing to the component, structure and morphology of the samples, play an important role to obtain the high discharge capacity and initial efficiency values.

Fig. 4 compares the rate capability for the $Li_{1+x}(Ni_{0.37}Mn_{0.63})_{1-x}O_2$ electrodes ($x = 0.123$, 0.111, 0.086, 0.031). After being charged at 0.2 C, the cells were discharged at 0.2 C, then discharged at 0.5, 1, 2, 3, 5 and 0.2 C in subsequent cycles. The results show that the rate performance of samples firstly increases and then decreases with the x value. $Li_{1.086}(Ni_{0.37}Mn_{0.63})_{0.914}O_2$

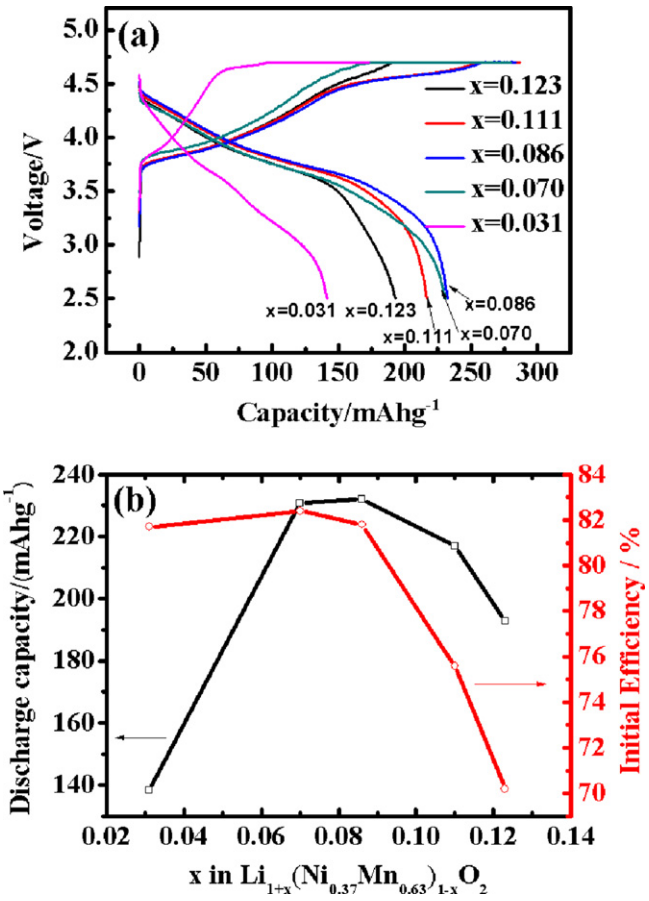

Fig. 3. (a) Initial charge/discharge voltage profiles of $Li_{1+x}(Ni_{0.37}Mn_{0.63})_{1-x}O_2$ electrodes (x = 0.123, 0.111, 0.086, 0.070, 0.031), and (b) the corresponding initial discharge capacity and initial efficiency values.

(x = 0.086) cell exhibits the best rate capability, which delivers the discharge capacity of 202.2 mAh g^{-1} at 0.5 C, 191.7 mAh g^{-1} at 1 C, 177.8 mAh g^{-1} at 2 C, 166.2 mAh g^{-1} at 3 C and 145.5 mAh g^{-1} at 5 C. Meanwhile, $Li_{1.031}(Ni_{0.37}Mn_{0.63})_{0.969}O_2$ (x = 0.031) electrode demonstrates an inferior performance at high rates, which is close related to its poor electronic conductivity induced by Ni-enriched impurity phases (Ni_6MnO_8) [29].

The long-term cycling performance and the median voltage of discharge (the potential corresponding to a half value of the discharge capacity) of $Li_{1+x}(Ni_{0.37}Mn_{0.63})_{1-x}O_2$ electrodes in the

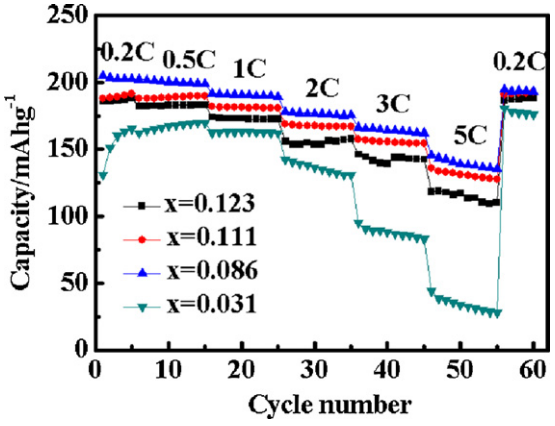

Fig. 4. Rate capability of the $Li_{1+x}(Ni_{0.37}Mn_{0.63})_{1-x}O_2$ electrodes (x = 0.123, 0.111, 0.086, 0.031) at different rates in the voltage range of 2.5–4.6 V.

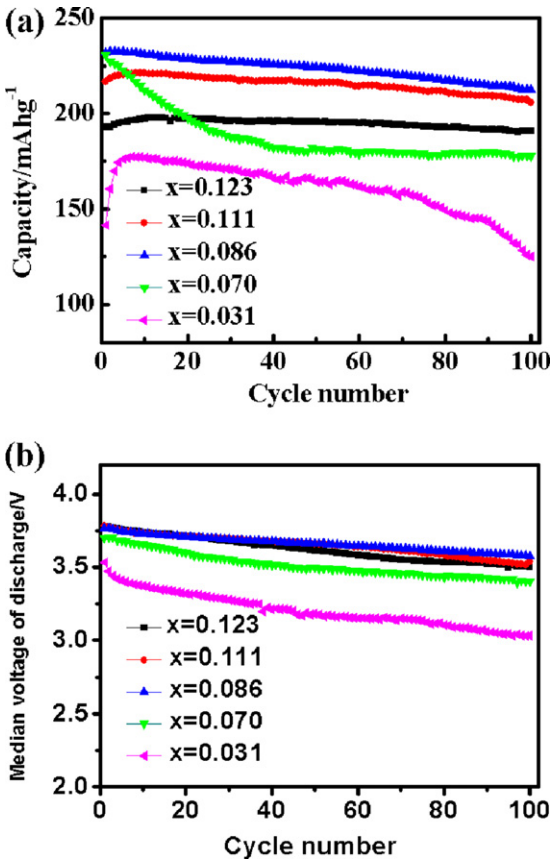

Fig. 5. (a) The cycling performance and (b) the median voltage of discharge of the $Li_{1+x}(Ni_{0.37}Mn_{0.63})_{1-x}O_2$ electrodes in the voltage range of 2.5–4.7 V, at 0.2 C (x = 0.123, 0.111, 0.086, 0.070, 0.031).

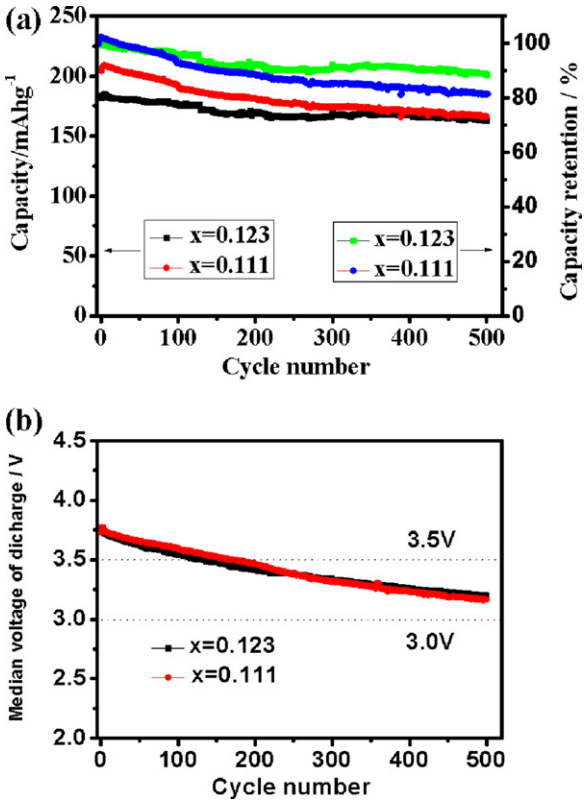

Fig. 6. (a) The long-term cycling performance and capacity retention and (b) the median voltage of discharge of the $Li_{1+x}(Ni_{0.37}Mn_{0.63})_{1-x}O_2$ electrodes in the voltage range of 2.5–4.7 V, at 0.5 C (x = 0.123, 0.111).

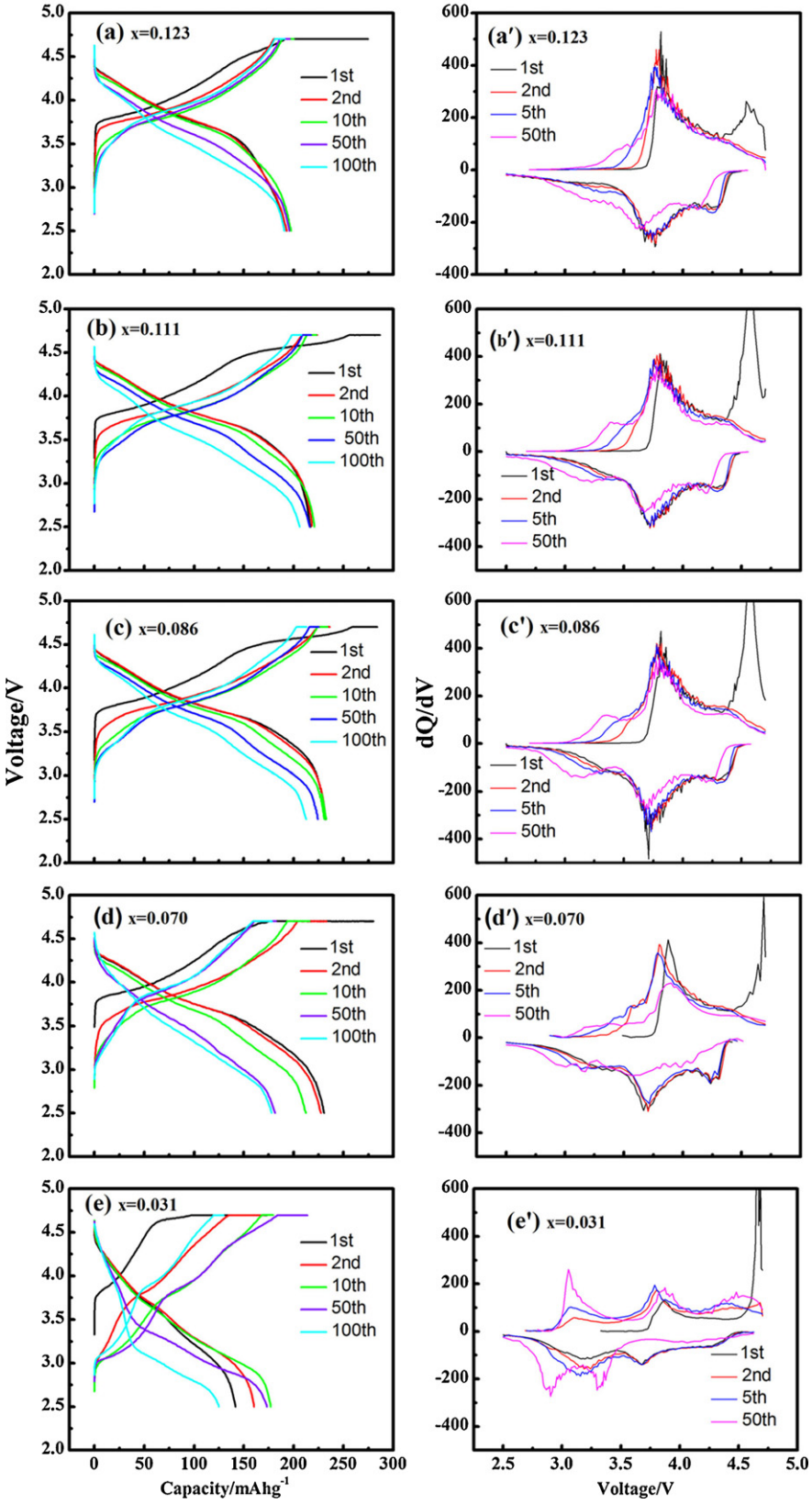

Fig. 7. Voltage profiles (left row) of the $Li_{1+x}(Ni_{0.37}Mn_{0.63})_{1-x}O_2$ (x = 0.123, 0.111, 0.086, 0.070, 0.031) electrodes during the 1st, 2nd, 10th, 50th and 100th cycles; The corresponding differential capacities vs. voltage plots (right row) of the 1st, 2nd, 5th and 50th cycles.

Table 2
The capacity retention and discharge capacity values of the $Li_{1+x}(Ni_{0.37}Mn_{0.63})_{1-x}O_2$ electrodes.

Samples	1st discharge capacity ($mAh\,g^{-1}$)	100th discharge capacity ($mAh\,g^{-1}$)	100 cycles capacity retention (%)
$x=0.123$	192.8	190.9	99
$x=0.111$	216.9	206.1	95
$x=0.086$	232.1	213.5	92
$x=0.070$	230.7	177.6	77
$x=0.031$	141.5	124.5	88

voltage range of 2.5–4.7 V at 0.2 C are shown in Fig. 5, and Table 2 summarizes the observed capacity and capacity retentions. It can be found that as the Li excessive value x increases from 0.031 to 0.123, the capacity retentions of the $Li_{1+x}(Ni_{0.37}Mn_{0.63})_{1-x}O_2$ cathodes are 88, 77, 92, 95 and 99%, after 100 cycles, of an initial capacity 141.5, 230.7, 232.1, 216.9 and 192.8 $mAh\,g^{-1}$, respectively. When the excessive lithium content increases, the amount of Li_2MnO_3-like component increases accordingly, and an appropriate amount of Li_2MnO_3 introduced into the structure would lead to structure stability and excellent cycling performance [18]. Although $Li_{1+x}(Ni_{0.37}Mn_{0.63})_{1-x}O_2$ with $x=0.086$ delivers a highest initial discharge capacity of 232.1 $mAh\,g^{-1}$, the capacity declines steadily upon cycling, whereas $Li_{1+x}(Ni_{0.37}Mn_{0.63})_{1-x}O_2$ with $x=0.123$ and $x=0.111$ electrodes show better cycle stability within 100 cycles. However, $Li_{1+x}(Ni_{0.37}Mn_{0.63})_{1-x}O_2$ electrodes with low Li excessive value, i.e. $x=0.070$ and $x=0.031$, show poor cycling performance, which may be due to the unstable composite structure, small primary particles, poor crystallinity, large polarization and Ni-enriched impurity phases (Ni_6MnO_8) in $Li_{1.031}(Ni_{0.37}Mn_{0.63})_{0.969}O_2$ sample ($x=0.031$). The medium discharge voltage of samples increases with an increase of Li content in the x rang of 0.031–0.086, and then decreases with an increase of Li content in the x rang of 0.086–0.123 (Fig. 5 (b)). $Li_{1+x}(Ni_{0.37}Mn_{0.63})_{1-x}O_2$ with $x=0.086$, 0.111, 0.123 deliver high median voltage of discharge above 3.5 V during 100 cycles, indicating the high energy output.

In order to further investigate the long-term cycling performance of $Li_{1+x}(Ni_{0.37}Mn_{0.63})_{1-x}O_2$ ($x=0.123$ and $x=0.111$) showing good cyclestability within 100 cycles, the cells were cycled at 0.5 C between 2.5 and 4.7 V for 500 cycles as shown in Fig. 6(a). It reveals that the 500th discharge capacities of $Li_{1.123}(Ni_{0.37}Mn_{0.63})_{0.877}O_2$ ($x=0.123$) and $Li_{1.111}(Ni_{0.37}Mn_{0.63})_{0.889}O_2$ ($x=0.111$) are 162.3 and 166.1 $mAh\,g^{-1}$, respectively, and the respective capacity retentions are about 89 and 81% of the initial discharge capacities of 183.3 and 204 $mAh\,g^{-1}$. However, these cathodes suffer from voltage decay on long-term cycling (500 cycles), which can be seen from Fig. 6(b). This phenomenon may be explained by the migration of manganese and nickel into the lithium layers upon cycling, resulting in a gradual transformation from the layered structure to a spinel-like phase [34], and the voltage decay lowers the energy output and efficiency of cell.

Further experiments and analysis were also performed to gain insight into the influence of lithium content on the discharge voltage plateau of $Li_{1+x}(Ni_{0.37}Mn_{0.63})_{1-x}O_2$ electrodes ($x=0.123$, 0.111, 0.086, 0.070, 0.031). The potential profiles of the 1st, 2nd, 10th, 50th and 100th cycles of $Li_{1+x}(Ni_{0.37}Mn_{0.63})_{1-x}O_2$ between 2.5 and 4.7 V at 0.2 C are shown in Fig. 7(a–e), where the corresponding differential capacities vs. voltage plots of the 1st, 2nd, 5th and 50th cycles are also shown in Fig. 9(a′–e′), respectively. There are obvious changes in the voltage profile with cycles. As the number of cycle increases, the discharge capacity above 3.5 V gradually decays, while the dQ/dV peak below 3.5 V shows an increase of magnitude following by a slightly shifts to lower voltage near 3 V, as presented before [34]. The deterioration performance as aforementioned become much more

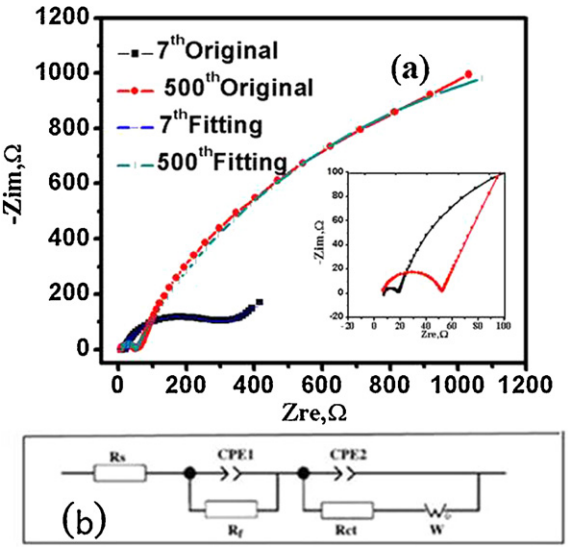

Fig. 8. (a) The original and fitting electrochemical impedance spectra curves of the $Li/Li_{1.111}(Ni_{0.37}Mn_{0.63})_{0.889}O_2$ cells after 7th cycles and 500th cycles. (b) The equivalent circuit adopted to fit impedance.

distinct with a decrease of Li content in $Li_{1+x}(Ni_{0.37}Mn_{0.63})_{1-x}O_2$ electrodes. The structural evolution appears associated with subsequent cycles, which does not necessarily accompany oxygen evolution during the first charging [34]. What is more, the structural evolution upon cycling can be inhibited with an increasing of x in $Li_{1+x}(Ni_{0.37}Mn_{0.63})_{1-x}O_2$. As previous reports on $zLi_2MnO_3\cdot(1-z)LiMeO_2$ solid solutions, high lithium content leads to high ratio of Li_2MnO_3 which play a vital role to stabilize the structure [30]. Therefore, the results confirmed that by introducing the appropriate amount of lithium content ($0.086 \leq x \geq 0.123$) into the series can suppress structural evolution during cycling and result in an excellent cycling performance.

The electrodes underwent 7 cycles between 2.5–4.7 V and then fully charged to 4.7 V. Considering that the contribution of anode to the cell resistance is minimal after 7 cycles and can be ignored, the charged cells rested for 10 h before EIS testing. The cells after 500 cycles were disassembled in the glove box and then the three-electrode cells were assembled with the used cathode as working electrode, and the fresh lithium foil as counter and reference electrode for an electrochemical impedance spectroscopy (EIS) analysis. The voltage values of the test cells were observed to be in a steady state before the EIS test, and the voltage drop was about 0.2 V. The corresponding Nyquist plots of $Li_{1.111}(Ni_{0.37}Mn_{0.63})_{0.889}O_2$ ($x=0.111$) after 7 and 500 cycles are given in Fig. 8, respectively. There are two semicircles in the diagram: the semicircle in the high frequency domain is ascribed to the passivating surface-film (solid electrolyte interface, SEI) on the cathode, while the other semicircle in the relatively low frequency region could simply be assigned to the charge transfer resistance (Rct). The calculated surface-film resistances of $Li_{1.111}(Ni_{0.37}Mn_{0.63})_{0.889}O_2$ ($x=0.111$) electrodes after 7 and 500 cycles are 10.8 and 45.8 Ω, respectively. While $Li_{1.111}(Ni_{0.37}Mn_{0.63})_{0.889}O_2$ ($x=0.111$) electrodes after 7 cycles exhibit a charge transfer resistance (Rct) of about 279.6 Ω. The charge transfer resistance (Rct) of the electrodes after 500 cycles becomes as large as 3240 Ω in our experiments (Table 3). The results show that the charge transfer resistance (Rct) of the Li-rich cathode materials increases obviously upon cycling, which plays a dominant role on the impedance parameter and electrochemical performance. Based on the previous reports about EIS [7,9], it can be found that once the voltages reach the plateau region between

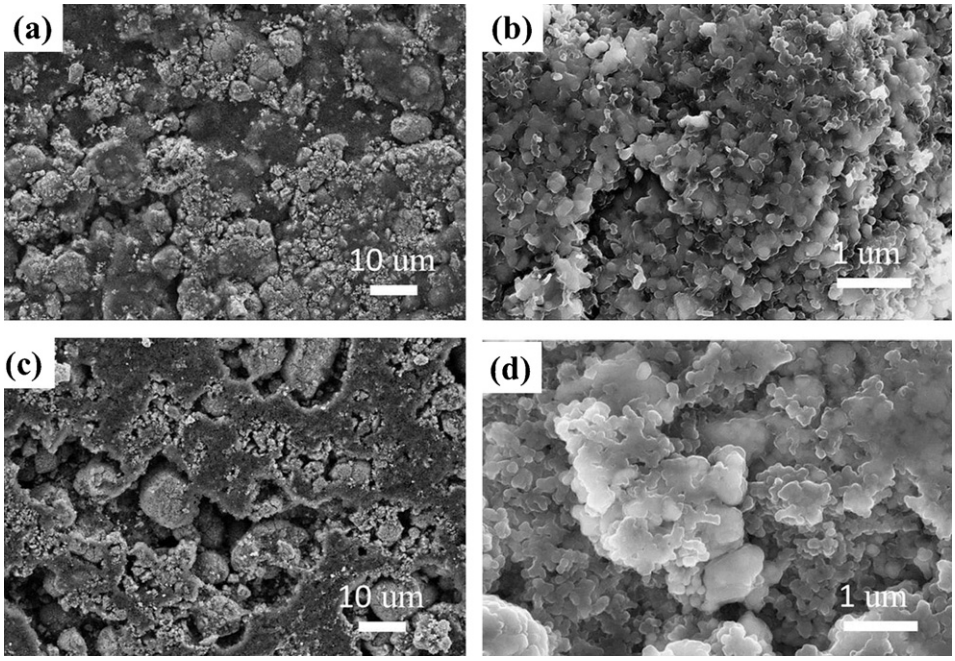

Fig. 9. SEM images of $Li_{1.111}(Ni_{0.37}Mn_{0.63})_{0.899}O_2$ elctrodes (a, b) before cycling and (c, d) after 500th cycles.

Table 3
Impedance parameters of $Li/Li_{1.111}(Ni_{0.37}Mn_{0.63})_{0.889}O_2$cell after 7th cycles and 500th cycles.

Cycle	Rs/Ω	Rf/Ω	Rct/Ω
7th	7.8	10.8	279.6
500th	6.1	45.8	3240.0

4.50 and 4.60 V, the major changes in the spectra is dominated by a significant increase of the charge transfer resistance (Rct). However, the charge transfer resistance (Rct) growth upon high voltage cycling is complex nature of the material system (e.g. various transport process overlap at high voltage), which needs further studies in the near future. The morphologies of the electrodes before and after 500 cycles are shown in Fig. 9. The fresh active material particles show homogeneous morphology and good contact with acetylene black, while the particles in the electrode after 500 cycles seem to be separated from acetylene black due to the presence of many voids between them. In addition, some primary particles show abnormal growth, which is one of the reasons leading to an increase of charge transfer resistance after long-term cycles. It's concluded that the charge-transfer resistance of the electrode increases significantly after long-term cycling which may lead from many factors including gradual structural transformation or worse interparticle contacts during cycling [35].

4. Conclusion

$Li_{1+x}(Ni_{0.37}Mn_{0.63})_{1-x}O_2$ with a fixed ratio of Mn:Ni = 0.63:0.37 but a different excessive lithium content have been prepared from co-precipitated $(Ni_{0.37}Mn_{0.63})CO_3$ precursor. These samples appear single phase with layered structure except $Li_{1.031}(Ni_{0.37}Mn_{0.63})_{0.969}O_2$ ($x = 0.031$), in which an additional phase Ni_6MnO_8 in the cubic rock-salt structure can be observed. All the samples retain a spherical morphology of the precursor. The primary particles tend to grow up and show clear boundaries with increasing lithium content. $Li_{1.086}(Ni_{0.37}Mn_{0.63})_{0.914}O_2$ ($x = 0.086$) expresses high initial efficiency of 82%, a high discharge capacity of 232 mAh g^{-1} at 0.2 C and a good rate capability, for example 145.5 mAh g^{-1} at 5 C. The series exhibits the capacity retention of 88, 77, 92, 95 and 99% of the initial discharge capacity after 100 cycles. Moreover, $Li_{1.123}(Ni_{0.37}Mn_{0.63})_{0.877}O_2$ ($x = 0.123$) and $Li_{1.111}(Ni_{0.37}Mn_{0.63})_{0.889}O_2$ ($x = 0.111$) operated at 0.5 C exhibit the capacity retention of 89%, and 81% after 500 cycles, respectively. Hence $Li_{1.086}(Ni_{0.37}Mn_{0.63})_{0.914}]O_2$ cathode material with large discharge capacity, low irreversible capacity, high median voltage of discharge, good rate capability and cycling performance is a promising material for the high power and high energy lithium ion batteries. Furthermore, the abnormal increase of the charge transfer resistance (Rct) at high voltage after long-term cycling leads to poor cycle performance of the series, which should be further studied in the near future

Acknowledgements

This work was financially supported by the National 863 Program of China (No. 2009AA03Z226), the Project on the Integration of Industry, Education and Research of Guangdong Province (No. 2011A090200012) and the Fundamental Research Funds for the Central Universities (No. FRF-MP-12-005B).

References

[1] K. Numata, C. Sakaki, S. Yamanaka, Synthesis of solid solutions in a system of $LiCoO_2$-Li_2MnO_3 for cathode materials of secondary lithium batteries, Chemistry Letters 8 (1997) 725.
[2] Y. Lee, M.G. Kim, J. Cho, Layered $Li_{0.88}[Li_{0.18}Co_{0.33}Mn_{0.49}]O_2$ nanowires for fast and high capacity Li-ion storage material, Nano Letters 8 (2008) 957.
[3] Y.J. Park, Y.S. Hong, X. Wu, M.G. Kim, K.S. Ryu, S.H. Chang, Synthesis and electrochemical characteristics of $Li[Co_xLi_{(1/3-x/3)}Mn_{(2/3-2x/3)}]O_2$ compounds, Journal of the Electrochemical Society 151 (2004) A720.
[4] Z. Lu, J.R. Dahn, Structure and electrochemistry of layered $Li[Cr_xLi_{(1/3-x/3)}Mn_{(2/3-2x/3)}]O_2$, Journal of the Electrochemical Society 149 (2002) A1454.
[5] T. Ohzuku, M. Nagayama, K. Tsuji, K. Ariyoshi, High-capacity lithium insertion materials of lithium nickel manganese oxides for advanced lithium-ion batteries: toward rechargeable capacity more than 300 mAh g^{-1}, Journal of Materials Chemistry 21 (2011) 10179.
[6] Z. Lu, J.R. Dahn, Understanding the anomalous capacity of $Li/Li[Ni_xLi_{(1/3-2x/3)}Mn_{(2/3-x/3)}]O_2$ cells using in situ X-ray diffraction and electrochemical studies, Journal of the Electrochemical Society 149 (2002) A815.

[7] B. Xu, C.R. Fell, M.F. Chi, Y.S. Meng, Identifying surface structural changes in layered Li-excess nickel manganese oxides in high voltage lithium ion batteries: a joint experimental and theoretical study, Energy and Environmental Science 4 (2011) 2223.
[8] W.C. West, J. Soler, B.V. Ratnakumar, Preparation of high quality layered-layered composite Li_2MnO_3–$LiMO_2$ (M = Ni, Mn, Co) Li-ion cathodes by a ball milling–annealing process, Journal of Power Sources 204 (2012) 200.
[9] S.K. Martha, J. Nanda, G.M. Veith, N.J. Dudney, Surface studies of high voltage lithium rich composition: $Li_{1.2}Mn_{0.525}Ni_{0.175}Co_{0.1}O_2$, Journal of Power Sources 216 (2012) 179.
[10] Z. Lu, D.D. MacNeil, J.R. Dahn, Layered cathode materials $Li[Ni_x\ Li_{(1/3-2x/3)}\ Mn_{(2/3-x/3)}]O_2$ for lithium-ion batteries, Electrochemical and Solid-State Letters 4 (2001) A191.
[11] Z. Lu, Z.H. Chen, J.R. Dahn, Lack of cation clustering in $Li[Ni_xLi_{1/3-2x/3}Mn_{2/3-x/3}]O_2$ ($0 < x \leq 1/2$) and $Li[Cr_xLi_{(1-x)/3}Mn_{(2-2x)/3}]O_2$ ($0 < x < 1$), Chemistry of Materials 15 (2003) 3214.
[12] Z. Lu, L.Y. Beaulieu, R.A. Donaberger, C.L. Thomas, J.R. Dahn, Synthesis, structure, and electrochemical behavior of $Li[Ni_xLi_{1/3-2x/3}Mn_{2/3-x/3}]O_2$, Journal of the Electrochemical Society 149 (2002) A778.
[13] J. Bareno, C.H. Lei, J.G. Wen, S.-H. Kang, I. Petrov, D.P. Abraham, Local structure of layered oxide electrode materials for lithium-ion batteries, Advanced Materials 22 (2010) 1122.
[14] A. van Bommel, L.J. Krause, J.R. Dahn, Investigation of the irreversible capacity loss in the lithium-rich oxide $Li[Li_{1/5}Ni_{1/5}Mn_{3/5}]O_2$ batteries and energy storage, Journal of the Electrochemical Society 158 (2011) A731.
[15] J. Liu, Q. Wang, B. Reeja-Jayan, A. Manthiram, Carbon-coated high capacity layered $Li[Li_{0.2}Mn_{0.54}Ni_{0.13}Co_{0.13}]O_2$ cathodes, Electrochemistry Communications 12 (2010) 750.
[16] J. Liu, A. Manthiram, Functional surface modifications of a high capacity layered $Li[Li_{0.2}Mn_{0.54}Ni_{0.13}Co_{0.\ 13}]O_2$ cathode, Journal of Materials Chemistry 20 (2010) 3961.
[17] A. Bommel, L.J. Krause, J.R. Dahn, Investigation of the irreversible capacity loss in the lithium-rich oxide $Li[Li_{1/5}Ni_{1/5}Mn_{3/5}]O_2$, Journal of the Electrochemical Society 158 (2011) A731.
[18] M.M. Thackeray, S.-H. Kang, C.S. Johnson, J.T. Vaughey, R. Benedek, S.A. Hackney, Li_2MnO_3-stabilized $LiMO_2$ (M = Mn, Ni, Co) electrodes for lithium-ion batteries, Journal of Materials Chemistry 17 (2007) 3112.
[19] A. Ito, D. Li, Y. Sato, M. Arao, M. Watanabe, M. Hatano, H. Horie, Y. Ohsawa, Cyclic deterioration and its improvement for Li-rich layered cathode material $Li[Ni_{0.17}Li_{0.2}Co_{0.07}Mn_{0.56}]O_2$, Journal of Power Sources 195 (2010) 567.
[20] N. Yabuuchi, K. Yoshii, S.-T. Myung, I. Nakai, S. Komaba, Detailed studies of a high-capacity electrode material for rechargeable batteries, Li_2MnO_3-$LiCo_{1/3}Ni_{1/3}Mn_{1/3}O_2$, Journal of the American Chemical Society 133 (2011) 4404.
[21] S.-H. Kang, C.S. Johnson, J.T. Vaughey, K. Amine, M.M. Thackeray, The effects of acid treatment on the electrochemical properties of $0.5Li_2MnO_3{\cdot}0.5LiNi_{0.44}Co_{0.25}Mn_{0.31}O_2$ electrodes in lithium cells, Journal of the Electrochemical Society 153 (2006) A1186.
[22] J. Gao, A. Manthiram, Eliminating the irreversible capacity loss of high capacity layered $Li[Li_{0.2}Mn_{0.54}Ni_{0.13}Co_{0.13}]O_2$ cathode by blending with other lithium insertion hosts J, Power Sources 191 (2009) 644.
[23] J. Gao, J. Kim, A. Manthiram, High capacity $Li[Li_{0.2}Mn_{0.54}Ni_{0.13}Co_{0.13}]O_2$-$V_2O_5$ composite cathodes with low irreversible capacity loss for lithium ion batteries, Electrochemistry Communications 11 (2009) 84.
[24] S.-H. Kang, M.M. Thackeray, Enhancing the rate capability of high capacity $xLi_2MnO_3{\cdot}(1-x)LiMO_2$ (M = Mn, Ni, Co) electrodes by Li-Ni-PO_4 treatment, Electrochemistry Communications 11 (2009) 748.
[25] J. Li, R. Klöpsch, M.C. Stan, S. Nowak, M. Kunze, M. Winter, S. Passerini, Synthesis and electrochemical performance of the high voltage cathode material $Li[Li_{0.2}Mn_{0.56}Ni_{0.16}Co_{0.08}]O_2$ with improved rate capability, Journal of Power Sources 196 (2011) 4821.
[26] A.L. Patterson, The Scherrer formula for X-ray particle size determination, Physical Review 56 (1939) 978.
[27] Y.S. Meng, G. Ceder, C.P. Grey, W.-S. Yoon, M. Jiang, J. Breger, Y. Shao-Horn, Cation ordering in layered O_3 $Li[Ni_xLi_{1/3-2x/3}Mn_{2/3-x/3}]O_2$ ($0 \leq x \leq 1/2$) compounds, Chemistry of Materials 17 (2005) 2386.
[28] N. Yabuuchi, Y.C. Lu, A.N. Mansour, S. Chen, Y. Shao-Horn, The influence of heat-treatment temperature on the cation distribution of $LiNi_{0.5}Mn_{0.5}O_2$ and its rate capability in lithium rechargeable batteries, Journal of the Electrochemical Society 158 (2011) A192.
[29] Z. Tang, Z. Wang, X. Li, W. Peng, Influence of lithium content on the electrochemical performance of $Li_{1+x}(Mn_{0.533}Ni_{0.233}Co_{0.233})_{1-x}O_2$ cathode materials, Journal of Power Sources 208 (2012) 237.
[30] T.A. Arunkumar, Y. Wu, A. Manthiram, Factors influencing the irreversible oxygen loss and reversible capacity in layered $Li[Li_{1/3}Mn_{2/3}]O_2$-$Li[M]O_2$ (M = $Mn_{0.5-y}Ni_{0.5-y}Co_{2y}$ and $Ni_{1-y}Co_y$) solid solutions, Chemistry of Materials 19 (2007) 3067.
[31] A.R. Armstrong, M. Holzapfel, P. Novak, C.S. Johnson, S.-H. Kang, M.M. Thackeray, P.G. Bruce, Demonstrating oxygen loss and associated structural reorganization in the lithium battery cathode $Li[Ni_{0.2}Li_{0.2}Mn_{0.6}]O_2$, Journal of the American Chemical Society 128 (2006) 8694.
[32] H. Deng, I. Belharouak, Y.K. Sun, K. Amine, $Li_xNi_{0.25}Mn_{0.75}O_y$ ($0.5 \leq x \leq 2$, $2 \leq y \leq 2.75$) compounds for high-energy lithium-ion batteries, Journal of Materials Chemistry 19 (2009) 4510.
[33] J. Wang, G. Yuan, M. Zhang, B. Qiu, Y. Xia, Z. Liu, The structure, morphology, and electrochemical properties of $Li_{1+x}Ni_{1/6}Co_{1/6}Mn_{4/6}O_{2.25+x/2}$ ($0.1 \leq x \leq 0.7$) cathode materials, Electrochimica Acta 66 (2012) 61.
[34] J. Hong, D.-H. Seo, S.-W. Kim, H. Gwon, S.-T. Oh, K. Kang, Structural evolution of layered $Li_{1.2}Ni_{0.2}Mn_{0.6}O_2$ upon electrochemical cycling in a Li rechargeable battery, Journal of Materials Chemistry 20 (2010) 10179.
[35] D. Li, Y. Kato, K. Kobayakawa, H. Noguchi, Y. Sato, Preparation and electrochemical characteristics of $LiNi_{1/3}Mn_{1/3}Co_{1/3}O_2$ coated with metal oxides coating, Journal of Power Sources 160 (2006) 1342.